Geophysical Research Letters

RESEARCH LETTER
10.1029/2025GL120855

# Multi-Century Projections of Dynamic Sea Level Based on an Updated Two-Layer Emulator

**Jin Xing[1,2], Jiacan Yuan[1,2], Chris Smith[3,4], and Dawei Li[5]**

[1]Department of Atmospheric and Oceanic Sciences & Institute of Atmospheric Sciences & CMA-FDU Joint Laboratory of Marine Meteorology, Fudan University, Shanghai, China, [2]Shanghai Key Laboratory of Ocean-land-atmosphere Boundary Dynamics and Climate Change, Fudan University, Shanghai, China, [3]Department of Water and Climate, Vrije Universiteit Brussel, Brussels, Belgium, [4]Energy, Climate and Environment Program, International Institute for Applied Systems Analysis (IIASA), Laxenburg, Austria, [5]School of Oceanography, Shanghai Jiao Tong University, Shanghai, China

**Abstract** Projections of dynamic sea level (DSL) are essential for understanding regional sea level change, yet the high computational cost of global climate models limits their use across diverse emissions scenarios and extended multi-century time horizons. Here we update a DSL emulator, built on fast and slow climate responses to radiative forcing, by update parameter configurations to align with the IPCC AR6 projections. The enhanced emulator produces global-scale DSL projections through 2300 under five scenarios, ranging from low to very high greenhouse-gas emissions (SSP1-2.6, SSP2-4.5, SSP3-7.0, SSP5-8.5) and including an overshoot pathway (SSP5-3.4-OS) not assessed in AR6 sea-level projections. Results indicate widespread DSL rise in the Northern Hemisphere, largest in the North Atlantic, while widespread decline in the Southern Hemisphere. Changes are amplified under higher-emission scenarios and exhibit a delayed response driven by slow deep-ocean responses. Under SSP5-3.4-OS, DSL evolution approaches SSP1-2.6 levels during the 23rd century—revealing reversibility under stringent mitigation.

**Plain Language Summary** In the context of a warming climate, sea-level rise poses major social, economic, and ecological threats to coastal regions worldwide. Yet sea level is not rising evenly across the globe. One important component of regional differences of sea level rise is known as dynamic sea level (DSL), which depends on redistributions of heat and mass by ocean and wind circulations. However, global climate models are too computationally expensive to simulate DSL across multiple emission pathways and centuries into the future. Here, we updated a DSL emulator that efficiently reproduces the long-term ocean response to greenhouse-gas forcing while remaining consistent with the latest IPCC AR6 projections. Using this tool, we estimate global DSL changes through the year 2300 under five scenarios, including one with overshoot carbon emission in the middle of 21st century. We find that DSL rise is strongest in the North Atlantic and continues for centuries even after emissions decline, reflecting the slow adjustment of the deep ocean. Under strong mitigation with carbon removal, regional DSL patterns can approach low-emission levels, suggesting that part of sea-level rise may be reversible.

**Key Points:**

- A two-layer DSL emulator is updated to align with the AR6 projections, and projects DSL to additional scenarios and extended time horizons
- DSL changes show a delayed response to radiative forcing change due to the thermal inertia of the deep ocean
- Under SSP5-3.4-OS, DSL evolution closely approaches SSP1-2.6 after 2,100, suggesting potential reversibility under strong mitigation

**Supporting Information:**

Supporting Information may be found in the online version of this article.

**Correspondence to:**

J. Yuan,
jcyuan@fudan.edu.cn

**Citation:**

Xing, J., Yuan, J., Smith, C., & Li, D. (2026). Multi-century projections of dynamic sea level based on an updated two-layer emulator. *Geophysical Research Letters*, *53*, e2025GL120855. https://doi.org/10.1029/2025GL120855

Received 23 NOV 2025
Accepted 5 MAR 2026

**Author Contributions:**

**Data curation:** Jin Xing, Jiacan Yuan (lead)
**Formal analysis:** Jin Xing
**Funding acquisition:** Jiacan Yuan
**Investigation:** Jin Xing
**Methodology:** Jin Xing, Jiacan Yuan
**Software:** Jin Xing, Dawei Li
**Supervision:** Jiacan Yuan
**Validation:** Jin Xing
**Visualization:** Jin Xing
**Writing – original draft:** Jin Xing, Jiacan Yuan (supporting)
**Writing – review & editing:** Jiacan Yuan (equal), Chris Smith, Dawei Li (equal)



## 1. Introduction

Sea level rise (SLR) is a major consequence of global warming and poses growing risks to coastal societies, making robust assessment of regional relative sea level (RSL) projections essential for adaptation planning. RSL changes are driven by a combination of global processes—including glacier and ice-sheet mass loss and ocean thermal expansion—as well as regional factors such as ocean dynamics, gravitational and deformational effects, and vertical land motion (Gregory et al., 2016, 2019; IPCC, 2021; Oppenheimer et al., 2019; Weeks et al., 2023). These interacting drivers produce spatially heterogeneous coastal hazards, underscoring the importance of probabilistic RSL projections for risk-informed adaptation and policy decisions (Kopp, Oppenheimer, et al., 2023).

Among the local drivers of RSL, the sea level changes associated with dynamic effects are also known as dynamic sea level (DSL). Ensembles of the Coupled Model Intercomparison Project Phase 6 (CMIP6) served as the primary tools in projecting DSL. However, running coupled global climate models (GCMs) is computationally expensive, limiting their use for probabilistic projections across multiple centuries and a broader range of emission scenarios. Most CMIP6 models simulate the future climate only to 2100, with only a few extending to 2300 (Smith et al., 2025). Moreover, the models that participate in a given CMIP6 experiment are not based on a

systematic design but rather on voluntary model participation. As many GCMs share structural similarities and the available models do not span the full spread of climate uncertainty, the CMIP6 ensemble represents an "ensemble of opportunity" rather than a true probabilistic distribution (Tebaldi & Knutti, 2007).

To overcome these limitations, simplified climate emulators have been developed to project GMSL and RSL evolution (Malagón-Santos et al., 2025; Nauels et al., 2025; Palmer et al., 2018; Yuan & Kopp, 2021). These computationally efficient tools can generate probabilistic, century- and global-scale projections with minimal computational cost. Using a two-layer energy balance model (Held et al., 2010), Palmer et al. (2018) emulated global mean thermosteric sea level rise (GMTSLR) and produced CMIP5-consistent projections up to 2300. To account for spatial distribution, pattern scaling techniques have been introduced into the regional sea level projections (Bilbao et al., 2015), relating local responses to global indicators such as global-mean near-surface atmospheric temperature (GSAT) under the assumption of stationary forcing-response relationships (Tebaldi & Arblaster, 2014).

While most previous studies use univariate pattern scaling approaches, Yuan and Kopp (2021) developed a bivariate pattern scaling emulator incorporating both fast (GSAT) and slow (deep-ocean temperature) climate responses. Their emulator couples the finite amplitude impulse response model (FaIR) (Millar et al., 2017; C. J. Smith et al., 2018) with the two-layer energy balance model. Including a reduced complexity carbon cycle, FaIR computes atmospheric $CO_2$ concentration, radiative forcing, and temperature from prescribed emissions and has been adopted by the Intergovernmental Panel on Climate Change (IPCC) Working Groups (WGs) I and III in the Sixth Assessment Report (AR6) as one of the four benchmark emulators (IPCC, 2021, 2022). The resulting two-layer framework reduces errors relative to univariate pattern-scaling approaches and captures the nonstationary relationship between dynamic sea level and radiative forcing pathways aligning with CMIP5 projections. Recently, Malagón-Santos et al. (2025) used a tri-variate pattern scaling approach based on a three-layer energy balance model.

Over recent years, the CMIP6 ensemble has superseded CMIP5 as the primary basis for global climate simulations, offering improved model diversity, updated forcings, and enhanced capability for projecting and analyzing future climate change (Eyring et al., 2016). CMIP6 models perform better than CMIP5 in reproducing ocean heat content, DSL patterns, associated zonal wind stress, and DSL climatology (Jin et al., 2023; Lyu et al., 2020, 2021). Building on these advances, CMIP6 served as the physical foundation for the projections of sterodynamic sea level (the sum of DSL and GMTSLR) in AR6, which were derived from the Framework for Assessing Changes To Sea-level (FACTS) sterodynamics module, which estimates changes based on the time-varying correlation structure between GMTSLR and DSL change in the CMIP6 multi-model ensemble, with temperature inputs taken from a two-layer energy balance model (Kopp, Garner, et al., 2023). However, the FACTS database provides only sterodynamic sea level projections and does not separate regional DSL and GMTSLR components. Moreover, it covers only the four SSP-RCP scenarios in Tier 1 (e.g., SSP1-2.6, SSP2-4.5, SSP3-7.0, SSP5-8.5) plus one scenario in Tier 2 (e.g., SSP1-1.9). It does not provide overshoot pathways (e.g., SSP5-3.4-OS), which represents a pathway in which delayed near-term mitigation leads to a temporary exceedance of climate targets, followed by rapid emissions reductions, allowing assessment of the sea-level responses under aggressive mitigation pathways (O'Neil et al., 2016). These highlight the need to update the DSL emulator—originally developed using CMIP5—to incorporate the advances from CMIP6 and AR6, and to extend its application to future regional sea level projections across a wider range of scenarios. We emphasize that this paper does not extend to the other sources of sea-level rise, namely mass changes in polar ice sheets and mountain glaciers, land water storage, and vertical land motion.

To reach this end, this study pursues two primary objectives: (a) update the emulator's configurations in line with CMIP6 and AR6 and evaluate its performance; (b) apply the updated emulator to project future DSL changes, with particular emphasis on extending beyond the time horizon and scenario coverage of AR6 simulations.

## 2. Data and Methods

### 2.1. Data

We use monthly mean output of three key variables—"zostoga" (GMTSLR), "tas" (GSAT), and "zos" (DSL)—in multiple CMIP6 scenarios, including pre-industrial control, historical, SSP1-2.6, SSP2-4.5, SSP3-7.0, and SSP5-8.5, and SSP5-3.4-OS. Only six CMIP6 models provide all three variables up to 2300 under both SSP1-2.6 and

SSP5-8.5 scenarios (Table S1 in Supporting Information S1). To avoid potential contamination of forced signals due to model drift, the long-term linear trend in DSL in the pre-industrial control simulation at each grid point is subtracted from modeled DSL in other scenarios (Gregory et al., 2019). Although internal climate variabilities still remain, but they are typically of much shorter timescales than the time span of combined historical and future scenarios (450 years), so we expect minimal impact in fitting parameters for the emulator. DSL anomalies are then calculated relative to the 1995–2014 climatology mean. For comparison, we also use sterodynamic sea level projections from IPCC AR6 obtained via the NASA/IPCC Sea Level Projections Tool (Fox-Kemper et al., 2021; Garner et al., 2021; Kopp, Garner, et al., 2023).

The projected emission inputs to FaIR are derived from the Reduced Complexity Model Intercomparison Project (RCMIP, Nicholls et al., 2020). Here we consider five future scenarios, including four Tier 1 scenarios and one overshoot scenario (SSP5-3.4-OS). In the overshoot scenario, radiative forcing follows SSP5-8.5 until 2040 and then declines rapidly under aggressive mitigation, reaching 3.4 W $m^{-2}$ by 2,100 (O'Neill et al., 2016; Riahi et al., 2017).

### 2.2. Upgrade of the Emulator Based on the CMIP6 and AR6 Framework

The two-layer DSL emulator consists of two main components (Figure S1 in Supporting Information S1). The first component is a simple climate model FaIR-2LM (Yuan & Kopp, 2021) which is driven by emissions under different scenarios and simulates the responses of climate system, represented by fast and slow temperature trajectories; The FaIR-2LM is constructed by replacing the temperature component of FaIR v1.3 (Smith et al., 2018) with a two-layer energy balance model including an efficacy parameter for deep ocean heat uptake (Geoffroy et al., 2013; Held et al., 2010; see more details in SI). As a physically based simple climate model, the FaIR-2LM represents the climate system in an aggregated manner and simulates both linear and nonlinear responses to external forcing through the governing energy-balance equations. For each emission scenario, distributions of global mean temperature anomalies in the upper layer ($T$) and the lower layer ($T_0$) are generated by driving the model with the corresponding emission trajectory.

The second key component generates the spatial responses of DSL anomalies to the external forcing by applying a bivariate pattern-scaling approach to the paired $T$ and $T_0$ produced by FaIR-2LM, following Yuan and Kopp (2021):

$$\mathrm{DSL}(t_i,x,y) = \alpha(x,y)\,T(t_i) + \beta(x,y)\,T_0(t_i) + b(x,y) + e(t_i,x,y) \quad (1)$$

where $x$ and $y$ denote longitudes and latitudes, and $t_i$ denotes the simulation years (1981–2300) under scenario $i$. The terms $\alpha$ and $\beta$ represent the fast and slow response patterns of DSL anomalies to upper- and deep-layer temperature changes, respectively, while $b$ and $e$ are the intercept and residual terms. The pattern-scaling approach has been widely used to deviate the forced responses of DSL changes from the internal variability (Bilbao et al., 2015; Malagón-Santos et al., 2025; Perrette et al., 2013; Yuan & Kopp, 2021). The DSL emulator is designed to project the spatial response of DSL to external forcing under different emission scenarios, assuming that the DSL responses to $T$ and $T_0$ are stationary across scenarios (Held et al., 2010), rather than explicitly representing internal variability, which is complex and inherently nonlinear.

We update the two-layer DSL emulator by adjusting the key parameters that regulate climate feedbacks and responses in FaIR-2LM to be consistent with IPCC AR6, and applying the $\alpha$-$\beta$ pairs derived from pattern scaling based on CMIP6 models. Specifically, the DSL projection emulator is constructed following these steps.

1. Following the approach of Yuan and Kopp (2021), we adjust the distribution of three key parameters in FaIR-2LM (i.e., climate feedback parameter λ, ocean heat uptake efficiency $\gamma$, and the factor of deep-ocean heat uptake $\gamma\varepsilon$) according to the assessed medians, standard deviations, and likely ranges reported in IPCC AR6 Chapters 7 and 9 (Table S2 in Supporting Information S1). Then, we draw 100,000 samples from the distribution of each parameter via Monte Carlo sampling. Subsequently, 10,000 parameter sets of λ-$\gamma$-$\gamma\varepsilon$ combinations are generated using Latin Hypercube sampling (Stein, 1987) to efficiently represent the joint multidimensional distribution of the three parameters.
2. For each scenario, the 10,000 parameter sets, together with the scenario-specific emission trajectories (Nicholls et al., 2020) are applied to the FaIR-2LM emulator to generate 10,000 realizations of paired upper- and deep-layer temperatures anomalies ($T$ and $T_0$, respectively).

3. We calculate thermosteric sea level (GMTSLR) using the simulated $T$ and $T_0$, together with the thermal expansion coefficient $\sigma = 0.113 \times 10^{-24}$ m J$^{-1}$ from Section 9.2.4.1 of AR6, following Kuhlbrodt and Gregory (2012):

$$\text{GMTSLR} = \sigma \times (C\Delta T + C_0 \Delta T_0) \quad (2)$$

1. To establish the pool of $\alpha$ and $\beta$ pairs, we apply the bivariate pattern scaling approach to each CMIP6 model by regressing simulated DSL against the corresponding pair of $T$ and $T_0$ trajectories. Specifically, for each CMIP6 model, the key parameters of FaIR-2LM (Forster et al., 2020; Table S3 in Supporting Information S1) were calibrated to reproduce the model's global-mean near-surface air temperature. The calibrated FaIR-2LM is then used to generate paired trajectories of upper- and deep-layer temperature anomalies ($T$ and $T_0$). Subsequently, DSL anomalies from each CMIP6 model are regressed against the corresponding $T$ and $T_0$ using a bivariate pattern-scaling approach. This procedure yields six pairs of regression coefficients (α and β), one from each CMIP6 model, for the period 1981–2300, forming a pool of slope pairs (Figures S2–S3 in Supporting Information S1). The α patterns from the six models consistently exhibit negative DSL anomalies over tropical oceans and a dipole structure in the Southern Ocean, associated with surface-layer warming. The β patterns display coherent negative anomalies over the Southern Ocean and positive anomalies over mid-to low-latitude Indian and Pacific Oceans associated with deep-layer warming.
2. The projections of future DSL anomalies relative to the baseline period are obtained by combining each pair of $T$ and $T_0$ from the 10,000 pairs of ($T$, $T_0$) trajectories with a randomly resampled $\alpha$ and $\beta$ pair from the slope-pair pool.

## 3. Results

### 3.1. Projecting Changes in Global Variables

We evaluated the emulator's performance in reproducing global-mean variables (GSAT and GMTSLR) for each CMIP6 model (Figures S4, S5 and Table S4 in Supporting Information S1). The emulator closely reproduces GSAT and GMTSLR for the majority of GCMs. Across the four scenarios, the mean root-mean-square errors (RMSEs) of the emulated GSAT relative to the corresponding GCM simulations are generally below 0.5 K, except for IPSL-CM6A-LR (all scenarios) and ACCESS-CM2 and MRI-ESM2-0 under SSP5-8.5, where RMSEs reach up to 0.72 K. Emulated GMTSLR agrees closely with that in GCMs (RMSEs $\leq$ 0.05 m). The discrepancies likely reflect differences among GCMs in their representation of physical processes and responses to external forcing, together with the emulator's inability to explicitly resolve important internal variability and climate feedbacks that are embedded in dynamical processes represented in GCMs.

The emulator's projections of GSAT and GMTSLR were compared with the median and 90% uncertainty ranges reported in IPCC AR6 WGI Chapters 4 and 9 (IPCC, 2021), shown in Figure 1. The uncertainty range of emulator projections nearly encompasses that of AR6 projections for both variables. The medians of GSAT projections by the emulator closely match medians of AR6 projections under scenarios of SSP3-7.0, SSP5-8.5, and SSP5-3.4-OS, while slightly higher than medians of AR6 projections under low-emission scenarios (SSP1-2.6 and SSP2-4.5) by the end of the 23rd century. The medians of GMTSLR projections by the emulator are slightly higher than the medians of AR6 projections by the end of the 21st century. These results indicate that the emulator effectively reproduces the projections of GSAT and GMTSLR, capturing the overall spread of and AR6 projections. Notably, the emulator also simulates future changes of GMTSLR under the overshoot scenario SSP5-3.4-OS, which is not included in AR6 sea-level projections, revealing the potential reversibility of surface warming and the delayed response of ocean thermal expansion.

### 3.2. Projecting Changes in Sterodynamic Sea Level

To evaluate the updated emulator, we project the sterodynamic sea level using the emulator and compared it with estimates from AR6 and CMIP6 GCMs (Figure 2; Figures S6 and S7 in Supporting Information S1). By the end of the 23rd century, medians of sterodynamic projections by the emulator generally fall between the median of AR6 projections and the median of 6 GCMs projections. The absolute differences between the emulator and either AR6 or GCMs are smaller than those between AR6 and GCMs except under SSP3-7.0 (Figure 2a). This indicates

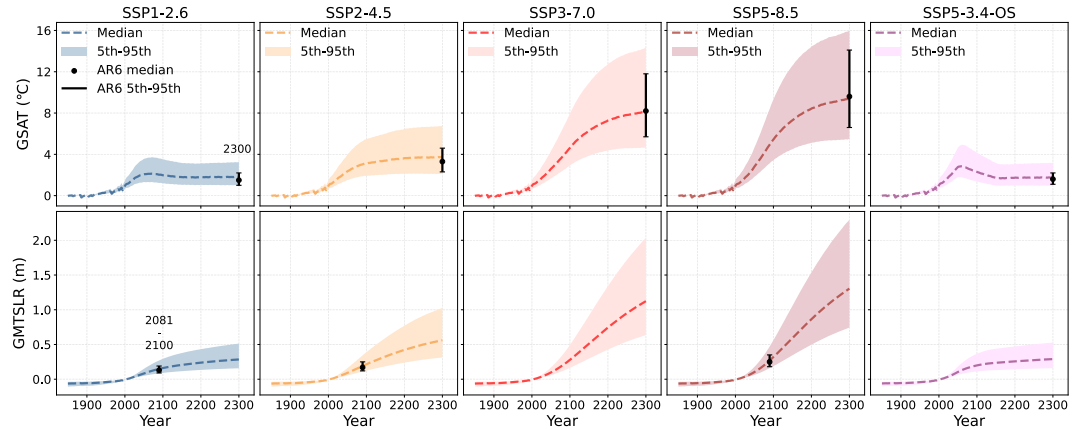


**Figure 1.** Ensemble projections of GSAT (upper panels) and GMTSLR (lower panels) changes relative to 1851–1900 and 1995–2014 baselines, respectively, under five scenarios. Shading denotes the 5th–95th uncertainty range of emulated projections, and colored bold dashed lines indicate the median. AR6 projections for GSAT in 2300 and for GMTSLR during 2081–2100 are shown as black error bars, overlaid on the emulator's projections for the corresponding periods.

smaller errors between the emulator and AR6 than errors between the GCM ensemble and AR6. The differences are largest under SSP3-7.0 among the four scenarios, likely because only one model (GISS-E2-1-G) was available for this scenario. Spatially, the differences between our emulator projections and the GCM ensemble are relatively uniform except at high latitudes. In contrast, discrepancies relative to AR6 exhibit pronounced spatial heterogeneity, with larger biases over the South Pacific, North Atlantic, Arctic, and Southern Oceans, likely reflecting the large uncertainties of ocean circulation over these regions.

To compare the temporal evolution of sterodynamic sea-level projections from the emulator with those from the CMIP6 ensemble and AR6, we selected two representative coastal locations: one in the western Pacific Ocean near Shanghai (31.5°N, 123°E), and the other in the eastern North Atlantic near Rotterdam (52.5°N, 3°E). Both are major coastal ports highly exposed to sea level rise under global warming. Emulator projections for 1981–2300 were compared with AR6 estimates and CMIP6 outputs (Figure 2b). For the location near Rotterdam, medians of emulator projection closely follow AR6 median under SSP1-2.6, SSP3-7.0, and SSP5-8.5, and align with GCMs but slightly lower than AR6 median under SSP2-4.5. For Shanghai, emulator medians remain consistent with those in AR6 across all scenarios over 1981–2300, with RMSEs below 0.04 m. At both sites, the emulator's 5th–95th percentile ranges encompass nearly all GCM projections under all four scenarios, and are slightly wider than the AR6 ranges under medium- and high-emission scenarios, but narrower under the low-emission case. Overall, the emulator can project sterodynamic sea level changes that encompass the uncertainty ranges of GCMs and are broadly consistent with AR6.

### 3.3. Projecting Changes in DSL

To isolate the spatial features of DSL from the sterodynamic sea-level changes, we separately analyzed the emulator-based DSL projections and their uncertainties. The emulator extends projections to 2300 for SSP2-4.5 and SSP3-7.0–missing from most CMIP6 models–as well as for SSP5-3.4-OS, which is not included in AR6 sea-level projections. During 2081–2100, DSL anomalies are projected to be negative over the southern Indian, southeastern Pacific, and Southern Oceans, while DSL shows positive anomalies in the northwest Pacific, Atlantic, and Arctic oceans, with larger magnitudes of DSL changes in higher emission scenarios (Figure S8 in Supporting Information S1). During 2281–2300, the spatial patterns of projected DSL anomalies are similar to those during 2081–2100 in four Tier 1 scenarios, except for larger magnitudes and uncertainty ranges (Figure 3). Under SSP5-3.4-OS, the projected DSL changes lie between those in SSP1-2.6 and SSP2-4.5 during 2081–2100. During 2281–2300, they are nearly identical to the projected pattern in SSP1-2.6 (Figure 3 and Figure S8 in Supporting Information S1).

To provide geographically representative projections, six locations were selected to examine the evolution of DSL in their vicinity (Figure 4 and Figure S9 in Supporting Information S1): Rotterdam on the northeastern Atlantic coast, Shanghai on the northwestern Pacific coast, New York City on the northwestern Atlantic coast,

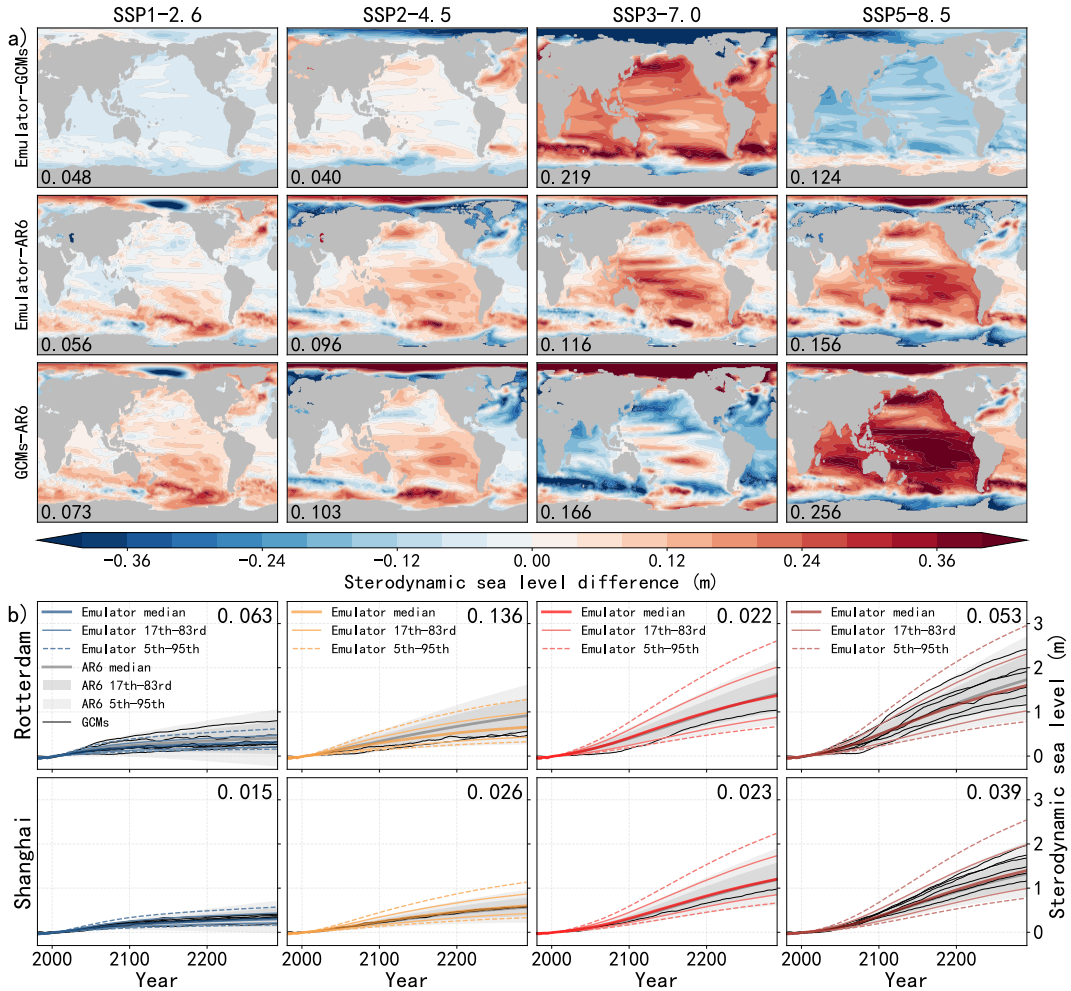


**Figure 2.** Comparison of sterodynamic sea level ensemble projections from AR6, CMIP6, and our emulator. (a) Median differences for 2281–2300 under four scenarios: emulator − CMIP6 (top), emulator − AR6 (middle), and CMIP6 − AR6 (bottom). Values in the lower-left corner denote the globally averaged absolute difference. (b) Projections for Rotterdam (upper) and Shanghai (lower). Colored lines show the emulator, gray line and shading show AR6, and thin black lines show CMIP6. Light shading or dashed colored lines indicate the 5th–95th percentile range; darker shading and solid lines indicate the 17th–83rd range.

Port of Abidjan on the Eastern Atlantic coast, the Maldives in the Indian Ocean, and Lima on the southeastern Pacific coast. For each site, the DSL at the nearest available ocean grid was projected through the 23rd century. The magnitude of the DSL rise is the largest near Rotterdam and New York City, both located in the Northern Atlantic. In contrast, projected DSL changes and associated uncertainties in the Southern Hemisphere are generally smaller, particularly relative to those in the North Atlantic. The DSL time series exhibit pronounced nonlinear trend after 2100, likely reflecting the emergence of the slow responses due to deep ocean spanning longer time scales. In the Northern Hemisphere, DSL evolution shows strong scenario-dependent differences. Notably, under SSP5-3.4-OS, DSL peaks around 2050 and subsequently converges toward the trajectory of SSP1-2.6 by the end of the 23rd century. In the Southern Hemisphere, the differences among medians of projections in different scenarios are very small, but the uncertainty range widens with increasing radiative forcing. Under SSP5-3.4-OS, both the median and spread remain close to those under SSP1-2.6 throughout the period.

These results highlight the potential reversibility of DSL changes and the delayed responses of DSL changes to radiative forcing due to the long-timescale adjustment of the deep ocean.

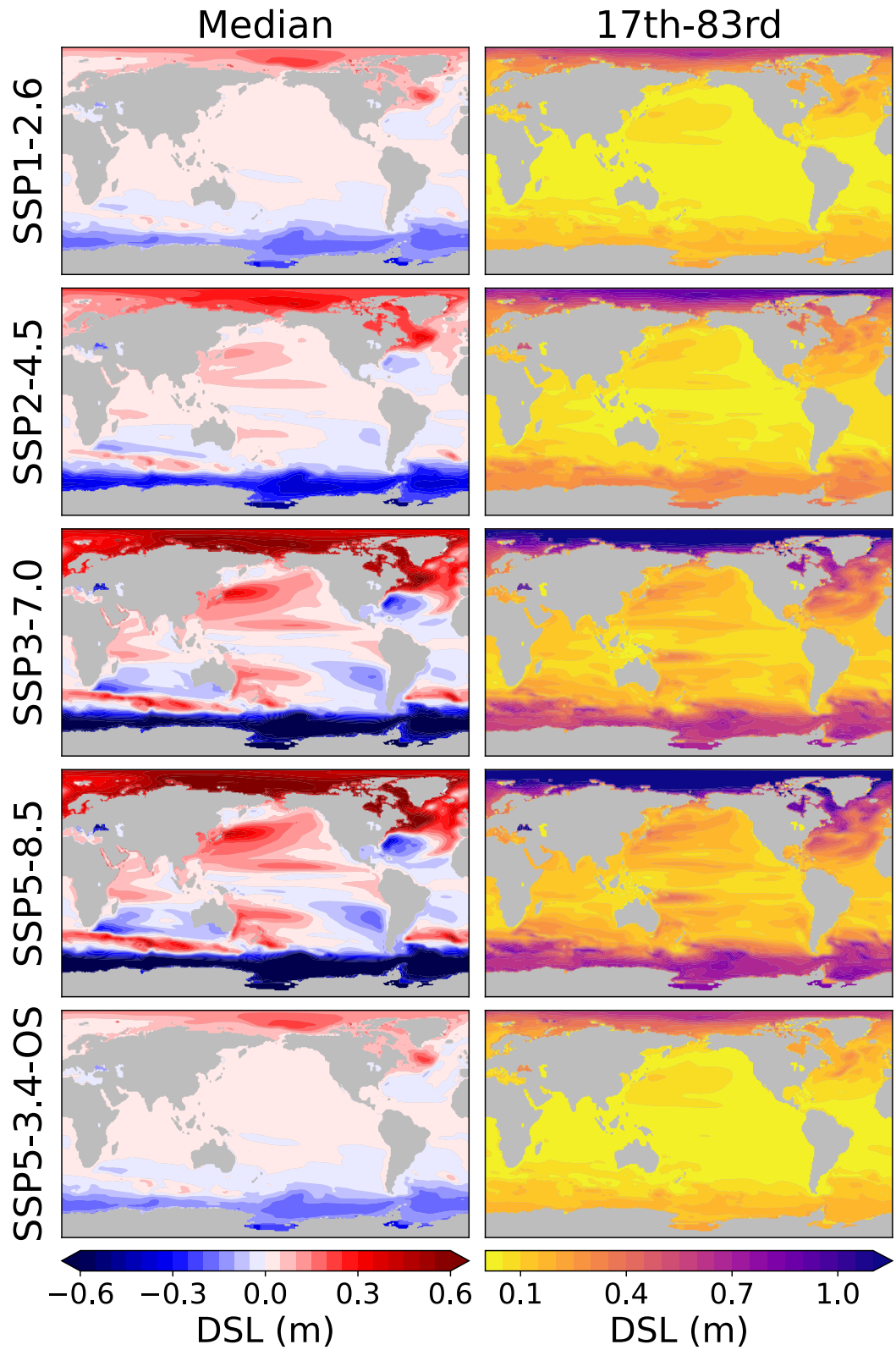


**Figure 3.** Median (left) and 17th–83rd percentile range (right) of DSL-changes projections under four scenarios over 2281–2300 relative to 1995–2014.

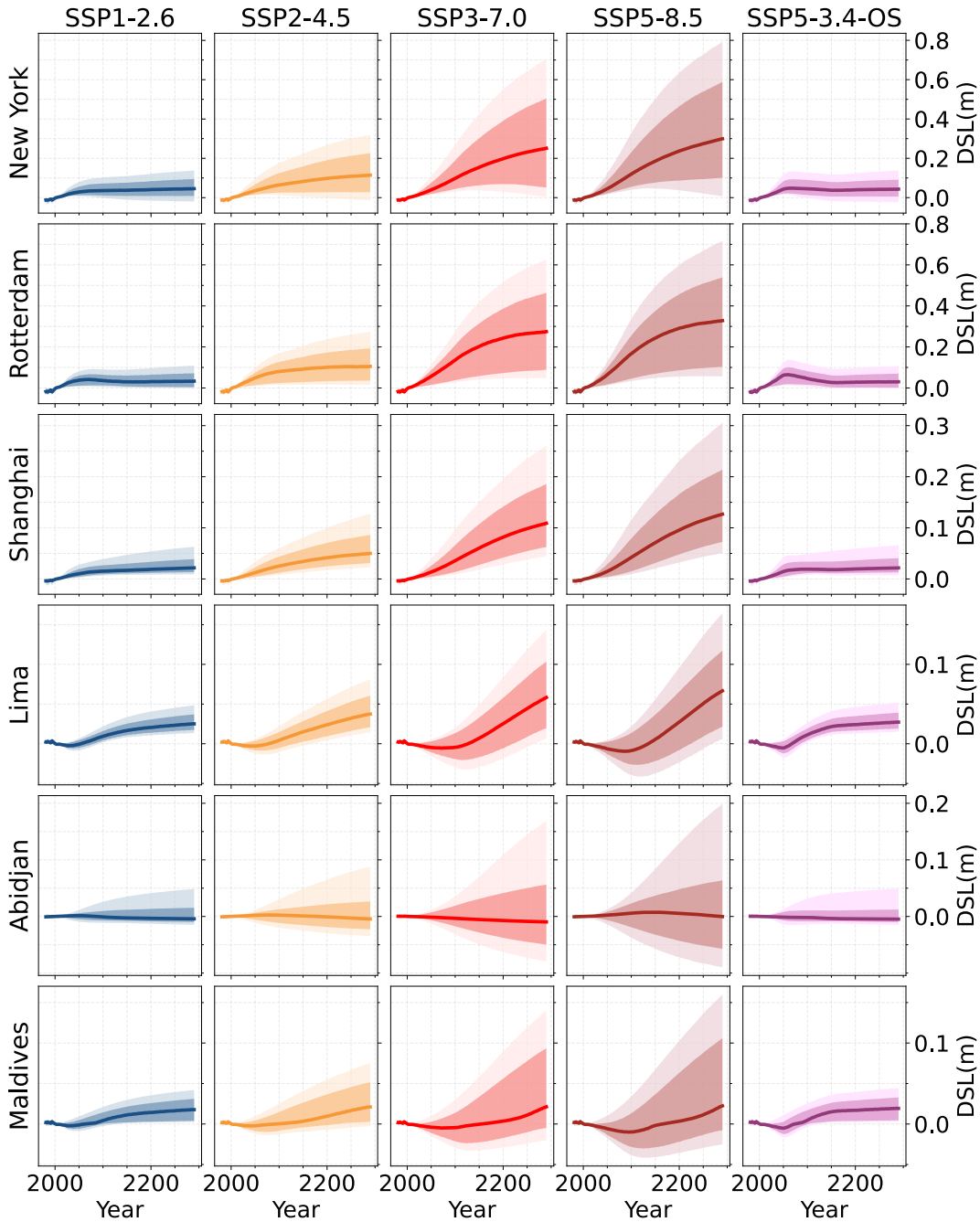


**Figure 4.** Emulator-based ensemble projections of DSL at six selected sites under five SSP scenarios, relative to 1995–2014. Colored bold lines denote medians, light shading shows the 5th–95th percentile range, and dark shading the 17th–83rd range.

## 4. Discussion and Conclusions

This study updates the two-layer DSL emulator with revised configurations and inputs consistent with AR6 and CMIP6 (Figure S1 in Supporting Information S1). Based on the updated emulator, we generate the projections of GSAT, GMTSLR, sterodynamic sea level, and DSL extending to 2300 across five scenarios (i.e., SSP1-2.6, SSP2-4.5, SSP3-7.0, SSP5-8.5, SSP5-3.4-OS). The emulator reproduces GSAT and GMTSLR trajectories from the corresponding CMIP6 models, with biases generally within 0.5 K and 0.03 m for most models, while larger deviations occur only in a limited subset (Table S4 in Supporting Information S1). It also captures both the spread

and median of the GSAT and GMTSLR projections across the available AR6 scenarios (Figure 1). The medians of emulated sterodynamic sea level projections fall between median estimates of the CMIP6 ensemble and those of AR6 projections, demonstrating robust and consistent performance (Figure 2a). Its 66% uncertainty range encompasses nearly all GCM projections, confirming the ability of the emulator to reproduce probabilistic sea-level outcomes (Figure 2b).

The updated emulator produces DSL projections that can be readily extended to additional emission pathways and longer time horizons not covered by current AR6 or GCM simulations (Figures 3 and 4). The emulated DSL projections exhibit pronounced spatial heterogeneity. Relative to 1995–2014, DSL increases over the Arctic, Kuroshio Extension, and North Atlantic Current, while decreasing over the Southern Ocean, with larger magnitudes under higher-emission scenarios (Figure 3). Sites along the coasts of the North Atlantic (e.g., near New York City and Rotterdam) are projected to face the largest DSL rise, whereas those in the Southern Hemisphere (e.g., near Lima, Abidjan, Maldives) show smaller increases and narrower uncertainties (Figure 4). After 2100, DSL projections display an apparent nonlinear trend, reflecting the slow responses of deep-ocean processes. Under SSP5-3.4-OS, DSL rise stabilizes after the middle of the 21st century, and converges toward SSP1-2.6 levels by the end of the 23rd century, underscoring the potential reversibility of sea-level change under stringent mitigation.

Although the emulator efficiently projects DSL across extended scenarios and time horizons, certain limitations remain. For instance, due to the coarse horizontal resolution (generally >100 km), CMIP6 models do not resolve the mesoscale and sub-mesoscale ocean processes, relying instead on parameterizations that cannot fully capture the dynamics of boundary currents, eddies, and fronts (Hewitt et al., 2020). This may introduce biases in the patterns of slopes used in generating the spatial projections of DSL. A three-layer energy balance model was also used to emulate DSL projections under CMIP6 scenarios (Malagón-Santos et al., 2025), offering additional parameter flexibility and enabling representation of the 10–20-year timescale—intermediate between fast (2–7 years) and slow (80–400 years) responses. However, since the performance of the two-layer and three-layer emulators is comparable, particularly under low-emission scenarios, we primarily use the two-layer emulator. This choice aligns with our focus on long-term DSL changes (extending to 300 years) and low-emission or carbon removal scenarios. Moreover, the two-layer model provides a clearer physical interpretation: the upper layer represents the atmosphere and ocean mixed layer, while the lower layer corresponds to the deep ocean. Nevertheless, the updated emulator provides spatially heterogeneous DSL projections with probabilistic uncertainty distributions that span multiple centuries, complementing CMIP6 and AR6 DSL projections with all the Tier 1 and an overshoot scenarios, as well as extended time horizons. After demonstrating the applicability to several SSP-RCP scenarios, the emulator can be applied to any emissions scenario (such as those resulting from integrated assessment models) to project regional DSL. These projections are particularly valuable for island nations and low-lying coastal regions vulnerable to sea level rise, where adaptation measures require substantial financial investments and long operational lifespans. Accordingly, policymakers are encouraged to adopt long-term perspectives rather than restricting planning to the next few decades (Malik & Ford, 2024; McEvoy et al., 2021; Tamura et al., 2019).

## Conflict of Interest

The authors declare no conflicts of interest relevant to this study.

## Availability Statement

The CMIP6 data are available from Earth System Grid Federation (ESGF) at https://esgf-node.llnl.gov/projects/cmip6/. AR6 sterodynamic sea-level projections are available at Garner et al. (2021). Emission inputs for FaIR are available at Z. Nicholls & Lewis (2021).

**Acknowledgments**
This research was supported by the Fundamental and Interdisciplinary Disciplines Breakthrough Plan of the Ministry of Education of China (NO. JYB2025XDXM911). D. L. was supported by the National Natural Science Foundation of China (Grant 42476263). We thank Prof. Robert E. Kopp for valuable discussions that improved the quality of this study. We thank the projection authors for developing and making the sea-level rise projections available, multiple funding agencies for supporting the development of the projections, and the NASA Sea Level Change Team for developing and hosting the IPCC AR6 Sea Level Projection Tool.

## References

Bilbao, R. A. F., Gregory, J. M., & Bouttes, N. (2015). Analysis of the regional pattern of sea level change due to ocean dynamics and density change for 1993–2099 in observations and CMIP5 AOGCMs. *Climate Dynamics*, *45*(9), 2647–2666. https://doi.org/10.1007/s00382-015-2499-z

Eyring, V., Bony, S., Meehl, G. A., Senior, C. A., Stevens, B., Stouffer, R. J., & Taylor, K. E. (2016). Overview of the coupled model intercomparison project phase 6 (CMIP6) experimental design and organization. *Geoscientific Model Development*, *9*(5), 1937–1958. https://doi.org/10.5194/gmd-9-1937-2016

Forster, P. M., Forster, H. I., Evans, M. J., Gidden, M. J., Jones, C. D., Keller, C. A., et al. (2020). Current and future global climate impacts resulting from COVID-19. *Nature Climate Change*, *10*(10), 913–919. https://doi.org/10.1038/s41558-020-0883-0

Fox-Kemper, B., Hewitt, H. T., Xiao, C., Aðalgeirsdóttir, G., Drijfhout, S. S., Edwards, T. L., et al. (2021). Ocean, Cryosphere and Sea level change. In V. Masson-Delmotte, P. Zhai, A. Pirani, S. L. Connors, C. Péan, S. Berger, et al. (Eds.), *Climate change 2021: The physical science Basis. Contribution of Working Group I to the sixth assessment report of the intergovernmental Panel on climate change*. Cambridge University Press. https://doi.org/10.1017/9781009157896.011

Garner, G. G., Hermans, T., Kopp, R. E., Slangen, A. B. A., Edwards, T. L., Levermann, A., et al. (2021). IPCC AR6 Sea Level Projections (version 20210809) [Dataset]. https://doi.org/10.5281/zenodo.5914709

Geoffroy, O., Saint-Martin, D., Olivié, D. J. L., Voldoire, A., Bellon, G., & Tytéca, S. (2013). Transient climate response in a two-layer energy-balance model. Part I: Analytical solution and parameter calibration using CMIP5 AOGCM experiments. *Journal of Climate*, *26*(6), 1841–1857. https://doi.org/10.1175/JCLI-D-12-00195.1

Gregory, J. M., Bouttes, N., Griffies, S. M., Haak, H., Hurlin, W. J., Jungclaus, J., et al. (2016). The Flux-Anomaly-Forced Model Intercomparison Project (FAFMIP) contribution to CMIP6: Investigation of sea-level and ocean climate change in response to $CO_2$ forcing. *Geoscientific Model Development*, *9*(11), 3993–4017. https://doi.org/10.5194/gmd-9-3993-2016

Gregory, J. M., Griffies, S. M., Hughes, C. W., Lowe, J. A., Church, J. A., Fukimori, I., et al. (2019). Concepts and terminology for Sea level: Mean, variability and change, both local and global. *Surveys in Geophysics*, *40*(6), 1251–1289. https://doi.org/10.1007/s10712-019-09525-z

Held, I. M., Winton, M., Takahashi, K., Delworth, T., Zeng, F., & Vallis, G. K. (2010). Probing the fast and slow components of global warming by returning abruptly to preindustrial forcing. *Journal of Climate*, *23*(9), 2418–2427. https://doi.org/10.1175/2009JCLI3466.1

Hewitt, H. T., Roberts, M., Mathiot, P., Biastoch, A., Blockley, E., Chassignet, E. P., et al. (2020). Resolving and parameterising the ocean mesoscale in Earth system models. *Current Climate Change Reports*, *6*(4), 137–152. https://doi.org/10.1007/s40641-020-00164-w

IPCC. (2021). *Climate change 2021: The physical science Basis. Contribution of Working Group I to the sixth assessment report of the intergovernmental Panel on climate change*. Cambridge University Press. https://doi.org/10.1017/9781009157896

IPCC. (2022). *Climate change 2022: Mitigation of climate Change. Contribution of Working Group III to the sixth assessment report of the intergovernmental Panel on climate change*. Cambridge University Press. https://doi.org/10.1017/9781009157926

Jin, C., Liu, H., & Lin, P. (2023). Evaluation of the seasonal to decadal variability in dynamic sea level simulations from CMIP5 to CMIP6. *Geoscience Letters*, *10*(1), 35. https://doi.org/10.1186/s40562-023-00291-w

Kopp, R. E., Garner, G. G., Hermans, T. H. J., Jha, S., Kumar, P., Reedy, A., et al. (2023). The Framework for Assessing Changes To Sea-level (FACTS) v1.0: A platform for characterizing parametric and structural uncertainty in future global, relative, and extreme sea-level change. *Geoscientific Model Development*, *16*(24), 7461–7489. https://doi.org/10.5194/gmd-16-7461-2023

Kopp, R. E., Oppenheimer, M., O'Reilly, J. L., Drijfhout, S. S., Edwards, T. L., Fox-Kemper, B., et al. (2023). Communicating future sea-level rise uncertainty and ambiguity to assessment users. *Nature Climate Change*, *13*(7), 648–660. https://doi.org/10.1038/s41558-023-01691-8

Kuhlbrodt, T., & Gregory, J. M. (2012). Ocean heat uptake and its consequences for the magnitude of sea level rise and climate change. *Geophysical Research Letters*, *39*(18). https://doi.org/10.1029/2012GL052952

Lyu, K., Zhang, X., & Church, J. A. (2020). Regional dynamic Sea level simulated in the CMIP5 and CMIP6 models: Mean biases, future projections, and their linkages. *Journal of Climate*, *33*(15), 6377–6398. https://doi.org/10.1175/JCLI-D-19-1029.1

Lyu, K., Zhang, X., & Church, J. A. (2021). Projected ocean warming constrained by the ocean observational record. *Nature Climate Change*, *11*(10), 834–839. https://doi.org/10.1038/s41558-021-01151-1

Malagón-Santos, V., Smith, C., Fredriksen, H.-B., Hermans, T. H. J., Edwards, T. L., & Slangen, A. B. A. (2025). Emulating long-term CMIP6 projections of sterodynamic sea-level change using a three-layer energy balance model. *Environmental Research Letters*, *20*(8), 084034. https://doi.org/10.1088/1748-9326/ade906

Malik, I. H., & Ford, J. D. (2024). Addressing the climate change adaptation gap: Key themes and future directions. *Climate*, *12*(2), 24. https://doi.org/10.3390/cli12020024

McEvoy, S., Haasnoot, M., & Biesbroek, R. (2021). How are European countries planning for sea level rise? *Ocean & Coastal Management*, *203*, 105512. https://doi.org/10.1016/j.ocecoaman.2020.105512

Millar, R. J., Nicholls, Z. R., Friedlingstein, P., & Allen, M. R. (2017). A modified impulse-response representation of the global near-surface air temperature and atmospheric concentration response to carbon dioxide emissions. *Atmospheric Chemistry and Physics*, *17*(11), 7213–7228. https://doi.org/10.5194/acp-17-7213-2017

Nauels, A., Nicholls, Z., Möller, T., Hermans, T. H. J., Mengel, M., Kloenne, U., et al. (2025). Multi-century global and regional sea-level rise commitments from cumulative greenhouse gas emissions in the coming decades. *Nature Climate Change*, *15*(11), 1198–1204. https://doi.org/10.1038/s41558-025-02452-5

Nicholls, Z., & Lewis, J. (2021). Reduced complexity model intercomparison project (RCMIP) protocol (v4.0.0) [Dataset]. *Zenodo*. https://doi.org/10.5281/zenodo.4589727

Nicholls, Z., Meinshausen, M., Lewis, J., Gieseke, R., Dommenget, D., Dorheim, K., et al. (2020). Reduced Complexity Model Intercomparison Project Phase 1: Introduction and evaluation of global-mean temperature response. *Geoscientific Model Development*, *13*(11), 5175–5190. https://doi.org/10.5194/gmd-13-5175-2020

O'Neill, B. C., Tebaldi, C., Van Vuuren, D. P., Eyring, V., Friedlingstein, P., Hurtt, G., et al. (2016). The scenario model intercomparison project (ScenarioMIP) for CMIP6. *Geoscientific Model Development*, *9*(9), 3461–3482. https://doi.org/10.5194/gmd-9-3461-2016

Oppenheimer, Glavovic, B., Hinkel, J., van Roderik, V., Magnan, A., Abd-Elgawad, A., et al. (2019). Sea level rise and implications for low lying Islands, coasts and communities. In *IPCC special report on the Ocean and Cryosphere in a changing climate* (pp. 321–445).

Palmer, M. D., Harris, G. R., & Gregory, J. M. (2018). Extending CMIP5 projections of global mean temperature change and sea level rise due to thermal expansion using a physically-based emulator. *Environmental Research Letters*, *13*(8), 084003. https://doi.org/10.1088/1748-9326/aad2e4

Perrette, M., Landerer, F., Riva, R., Frieler, K., & Meinshausen, M. (2013). A scaling approach to project regional sea level rise and its uncertainties. *Earth System Dynamics*, *4*(1), 11–29. https://doi.org/10.5194/esd-4-11-2013

Riahi, K., Van Vuuren, D. P., Kriegler, E., Edmonds, J., O'Neill, B. C., Fujimori, S., et al. (2017). The shared socioeconomic pathways and their energy, land use, and greenhouse gas emissions implications: An overview. *Global Environmental Change*, *42*, 153–168. https://doi.org/10.1016/j.gloenvcha.2016.05.009

Smith, C., Ramme, L., Wells, C. D., Gjermundsen, A., Li, H., Ilyina, T., et al. (2025). Overshoot and (ir) reversibility to 2300 in two $CO_2$-emissions driven earth system models. *EGUsphere*, 1–24. https://doi.org/10.5194/egusphere-2025-5292

Smith, C. J., Forster, P. M., Allen, M., Leach, N., Millar, R. J., Passerello, G. A., & Regayre, L. A. (2018). FAIR v1.3: A simple emissions-based impulse response and carbon cycle model. *Geoscientific Model Development*, *11*(6), 2273–2297. https://doi.org/10.5194/gmd-11-2273-2018

Stein, M. (1987). Large sample properties of simulations using Latin hypercube sampling. *Technometrics*, *29*(2), 143–151. https://doi.org/10.1080/00401706.1987.10488205

Tamura, M., Kumano, N., Yotsukuri, M., & Yokoki, H. (2019). Global assessment of the effectiveness of adaptation in coastal areas based on RCP/SSP scenarios. *Climatic Change*, *152*(3), 363–377. https://doi.org/10.1007/s10584-018-2356-2

Tebaldi, C., & Arblaster, J. M. (2014). Pattern scaling: Its strengths and limitations, and an update on the latest model simulations. *Climatic Change*, *122*(3), 459–471. https://doi.org/10.1007/s10584-013-1032-9

Tebaldi, C., & Knutti, R. (2007). The use of the multi-model ensemble in probabilistic climate projections. *Philosophical Transactions of the Royal Society A: Mathematical, Physical and Engineering Sciences*, *365*(1857), 2053–2075. https://doi.org/10.1098/rsta.2007.2076

Weeks, J. H., Fung, F., Harrison, B. J., & Palmer, M. D. (2023). The evolution of UK sea-level projections. *Environmental Research Communications*, *5*(3), 032001. https://doi.org/10.1088/2515-7620/acc020

Yuan, J., & Kopp, R. E. (2021). Emulating Ocean Dynamic Sea level by two-layer pattern scaling. *Journal of Advances in Modeling Earth Systems*, *13*(3), e2020MS002323. https://doi.org/10.1029/2020MS002323

## References From the Supporting Information

Bi, D., Dix, M., Marsland, S., O'Farrell, S., Sullivan, A., Bodman, R., et al. (2020). Configuration and spin-up of ACCESS-CM2, the new generation australian community climate and Earth system simulator coupled model. *Journal of Southern Hemisphere Earth Systems Science*, *70*(1), 225–251. https://doi.org/10.1071/ES19040

Boucher, O., Servonnat, J., Albright, A. L., Aumont, O., Balkanski, Y., Bastrikov, V., et al. (2020). Presentation and evaluation of the IPSL-CM6A-LR climate model. *Journal of Advances in Modeling Earth Systems*, *12*(7), e2019MS002010. https://doi.org/10.1029/2019MS002010

Forster, P., Storelvmo, T., Armour, K., Collins, W., Dufresne, J.-L., Frame, D., et al. (2021). The Earth's energy budget, climate feedbacks, and climate sensitivity. In V. Masson-Delmotte, P. Zhai, A. Pirani, S. L. Connors, C. Péan, S. Berger, et al. (Eds.), *Climate change 2021: The physical science Basis. Contribution of Working Group I to the sixth assessment report of the intergovernmental Panel on climate change*. Cambridge University Press. https://doi.org/10.1017/9781009157896.009

Kelley, M., Schmidt, G. A., Nazarenko, L. S., Bauer, S. E., Ruedy, R., Russell, G. L., et al. (2020). GISS-E2.1: Configurations and climatology. *Journal of Advances in Modeling Earth Systems*, *12*(8), e2019MS002025. https://doi.org/10.1029/2019MS002025

Yukimoto, S., Kawai, H., Koshiro, T., Oshima, N., Yoshida, K., Urakawa, S., et al. (2019). The meteorological research institute earth system model version 2.0, MRI-ESM2.0: Description and basic evaluation of the physical component. *Journal of the Meteorological Society of Japan. Ser. II, advpub.*, *97*(5), 931–965. https://doi.org/10.2151/jmsj.2019-051

Ziehn, T., Chamberlain, M. A., Law, R. M., Lenton, A., Bodman, R. W., Dix, M., et al. (2020). The australian earth system model: ACCESS-ESM1.5. *Journal of Southern Hemisphere Earth Systems Science*, *70*(1), 193–214. https://doi.org/10.1071/ES19035